PHYSICAL REVIEW B VOLUME 28, NUMBER 9 1 NOVEMBER 1983

Vortices in rotating superfluid ^{3}He-A

A. L. Fetter
Institute of Theoretical Physics, Department of Physics, Stanford University, Stanford, California 94305

J. A. Sauls and D. L. Stein
Joseph Henry Laboratories of Physics, Princeton University, Princeton, New Jersey 08544
(Received 10 June 1983)

We investigate the properties of rotating ^{3}He-A in the absence of a magnetic field. For fast rotating ^{3}He-A ($\Omega \gg \Omega_{c1}$) we find a transition from the type-I lattice of nonsingular vortex textures discussed by Fujita *et al.* to a lattice of singular 2π vortex textures with polar cores at a rotation speed of $\Omega = (\hbar/2m_3)(3L_D)^{-2} \simeq 32$ rad/sec for $T \simeq T_c$. A second transition to a lattice of singular vortices occurs at a much higher rotational speed $\Omega \simeq 10^{-1}\Omega_{c2}$. We also discuss ion mobility and sound attenuation in these vortex textures.

I. INTRODUCTION

The equilibrium state of an infinite stationary superfluid is a uniform order parameter, while configurations with either continuous variation of the order parameter or singular defects have higher energy. In this context, rotation plays an interesting role because the equilibrium state of a rotating superfluid typically contains one or more singularities associated with the finite angular momentum. These ideas are familiar in connection with superfluid ^{4}He, where the defects are quantized vortex lines with a core of radius of order the coherence length ξ. Although these vortices can, in principle, have multiple circulation, energy considerations favor single quantization. The resulting equilibrium state of a rotating superfluid in a cylinder of radius R depends on the angular speed Ω. For low angular speed, the superfluid remains at rest. At a critical value $\Omega_{c1} \approx (\hbar/m_4 R^2)\ln(R/\xi)$, a singly quantized vortex first appears; for larger angular speeds, superfluid ^{4}He rotates by forming an array of these quantized vortices. This situation persists up to a second critical value $\Omega_{c2} \approx \hbar/m_4\xi^2$, when the cores start to overlap. Since ξ is very small for ^{4}He($\xi \approx$ Å), Ω_{c2} is unattainably high ($\approx 10^{12}$ rad/sec); in contrast, Ω_{c1} is very low ($\approx 3\times 10^{-3}$ rad/sec for $R = 1$ cm). Thus most experiments deal with intermediate speeds, $\Omega_{c1} \ll \Omega \ll \Omega_{c2}$.

The analogous situation for ^{3}He is less understood because its order parameter is more complicated. In particular, dipole-locked ^{3}He-A has only a single topologically stable type of line singularity associated with one quantum of circulation.[1,2] Higher circulation states are topologically equivalent to configurations with lower circulation, but an energy barrier may intervene. One of the simplest nonsingular textures with circulation is a doubly quantized (4π) vortex, first studied by Anderson and Toulouse (AT).[3] In principle, rotating ^{3}He could contain an array of these textures, but other nonsingular configurations turn out to have lower free energy.[4]

The equilibrium state of nonrotating ^{3}He-A in a cylinder was first studied by Mermin and Ho (MH), who constructed a nonsingular texture with a single unit of circulation at the outer boundary.[5,6] At a critical angular speed $\Omega_{c1} \approx 10(\hbar/2m_3R^2)$, the equilibrium texture changes to one with three units of circulation at the outer wall, but remains nonsingular throughout the cylinder.[7] For somewhat higher angular speed, the detailed sequence of states is not known, but the situation becomes simpler when the total number of circulation quanta is large, because the effect of the cylinder boundary can be omitted. At moderate rotation speeds, a square array of nonsingular textures, similar to those studied by MH, is believed to have the lowest free energy.[4] For very high rotational speeds $\Omega \approx \Omega_{c2} \equiv \hbar/8m_3\xi^2$, where ξ is the temperature-dependent Ginzburg-Landau coherence length, and for $T \approx T_c$, Schopohl[8] finds that the minimum-energy configuration is a triangular lattice of singular vortices with the order parameter having either the axial or polar form. Comparison of these two limits implies that a transition must occur from nonsingular to singular vortices at some intermediate angular speed.

This paper addresses the question: What is the sequence of states in rotating ^{3}He-A for $\Omega_{c1} \ll \Omega \ll \Omega_{c2}$ and zero magnetic field? This limit is both theoretically tractable, because the density of vortices is large so that boundary effects can be ignored, and experimentally accessible, because Ω_{c1} is comparable with that for ^{4}He, whereas Ω_{c2} is very large ($\Omega_{c2} \approx 3\times 10^6$ rad/sec for $\xi = 0.03$ μm and $T/T_c \simeq 0.9$). Section II describes the general properties of vortices in the A phase and how they can be combined to form a regular array. The free energy of various possible configurations is considered in Sec. III. A comparison of the free energy of these configurations determines the angular speeds where textural transitions occur. In particular, we find that a nonsingular array is energetically favored when $\Omega < \hbar/18m_3L_D^2 \simeq 32$ rad/sec, where L_D is the characteristic dipole length, and that either of two distinct singular vortices can occur depending on the angular speed. In Sec. IV we discuss ion mobility and sound propagation in rotating ^{3}He-A, and suggest that ion-pulse shapes and sound attenuation measurements can

distinguish between the possible zero-field vortex-texture lattices.

II. GENERAL PROPERTIES OF VORTICES

The general features of vortices in superfluid ^{3}He-A are best understood in comparison with those of ^{4}He. We first review the situation for the simpler superfluid.

A. Vortices in superfluid ^{4}He II

The order parameter of liquid ^{4}He is a complex scalar function, $\Psi(\vec{r})=|\Psi(\vec{r})|e^{iS(\vec{r})}$. Spatial variations involve an energy density proportional to $|\vec{\nabla}\Psi|^2$, and the most important part comes from gradients of the phase $(\vec{\nabla}S)^2$ because variations in $|\Psi|$ are generally more costly in energy. Thus the order parameter for superfluid ^{4}He effectively reduces to a scalar phase function S. Its gradient is related to the superfluid velocity[9]

$$\vec{v}_s=\vec{\nabla}S\ . \tag{1}$$

Since $\Psi(\vec{r})$ is single valued, the phase S can change only by an integral multiple of 2π on going around any closed contour C. As a result, we obtain the well-known quantization of superfluid circulation

$$\oint_C \vec{v}_s\cdot d\vec{s}=2\pi p,\quad p=0,\pm1,\pm2,\ldots\ . \tag{2}$$

Equivalently, p is the winding number of the phase; if $p\neq0$, then there must be a singularity in $S(\vec{r})$ somewhere inside C.

The simplest case is to have

$$S(\vec{r})=p\phi+S_0\ , \tag{3}$$

where ϕ is the azimuthal angle in cylindrical polar coordinates, and S_0 is a constant. The corresponding superfluid velocity is

$$\vec{v}_s=(p/r)\hat{\phi}\ , \tag{4}$$

representing a p-fold quantized vortex line on the axis of symmetry. Although closed velocity streamlines are the most common way to visualize a vortex, it is often more instructive to consider the phase S directly by drawing a field of unit vectors oriented at the local angle S with respect to some fixed direction. This approach focuses directly on p as the winding number; Fig. 1 illustrates various possibilities for $p=\pm1$. Note that all three cases for $p=1$ have the same superfluid velocity, even though they look quite different.

The energy per unit length of a vortex is obtained by integrating the kinetic energy density $f=\frac{1}{2}\rho_s v_s^2$ to give $\pi\rho_s p^2\ln(a/\xi)$. The logarithmic divergence is cut off at the core radius ξ and at a large distance a, which is either the size of the container or the intervortex spacing. The logarithmic factor reflects the singularity in the phase function which forces a defect in the order parameter; $|\Psi|$ must be decreased to zero inside the core, $r\lesssim\xi$.

It is evident that a vortex represents an excited state of the system at rest, but it can be made the true thermodynamic equilibrium state merely by rotating the container appropriately. If the walls rotate with constant angular velocity $\vec{\Omega}$, then the normal fluid executes solid-body rotation with $\vec{v}_n=m_4\hbar^{-1}\vec{\Omega}\times\vec{r}$, and the free-energy density in the rotating frame is

$$\tilde{f}=f-m_4\hbar^{-1}\vec{\Omega}\cdot(\vec{r}\times\vec{j})\ , \tag{5a}$$

where f includes the normal-fluid kinetic energy density $\frac{1}{2}\rho_n v_n^2$ and

$$\vec{j}=\rho_s\vec{v}_s+\rho_n\vec{v}_n \tag{5b}$$

is the total current. Simple manipulations allow us to rewrite $\tilde{f}$ as

$$\tilde{f}=\tfrac{1}{2}\rho_s(\vec{v}_s-\vec{v}_n)^2-\tfrac{1}{2}\rho v_n^2\ , \tag{6}$$

where the last term is a constant that depends only on the angular speed and the shape of the container and will be omitted from here on. Thus, thermodynamic equilibrium is obtained by minimizing the mean-square superfluid velocity in the rotating frame, namely $(\vec{v}_s-\vec{v}_n)^2$.

Since $\mathrm{curl}\,\vec{v}_s=0$, except at singularities, whereas $\mathrm{curl}\,\vec{v}_n=2m_4\vec{\Omega}/\hbar$, $\vec{v}_s-\vec{v}_n$ cannot vanish identically. Nevertheless, the superfluid can mimic solid-body rotation by forming a uniform array of rectilinear vortices parallel to the rotation axis.[10] If C is a contour in the plane perpendicular to Ω enclosing N_c vortices in an area A_c, then Eqs. (1) and (2) show that

$$\oint_C \vec{v}_s\cdot ds=2\pi pN_c\ . \tag{7}$$

To minimize $(\vec{v}_s-\vec{v}_n)^2$ on the average, we require that Eq. (7) also equals the line integral of $\vec{v}_n$ around C; Stokes's theorem then gives the mean vortex density

$$N_c/A_c=m_4\Omega/\pi p\hbar\ . \tag{8}$$

For an angular speed $\Omega=1$ rad/sec, the vortex density is $N_c/A_c\approx2000\ \mathrm{cm}^{-2}$.

The preceding considerations assume only a uniform vortex density and are independent of the precise arrangement of the vortices. It is useful to consider the specific case of a lattice of rectilinear vortices parallel to $\hat{z}$ and intersecting the xy plane at the points $\vec{r}_{mn}=m\vec{b}_1+n\vec{b}_2$, where m and n are integers and $\vec{b}_1$ and $\vec{b}_2$ are elementary lattice vectors. Tkachenko[11] has studied the phase function for such an array, which we shall denote $\Phi(\vec{r})$. It

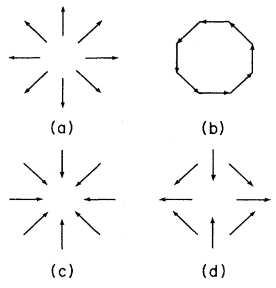

FIG. 1. Phase-angle representation of vortices. (a), (b), and (c) all represent $p=+1$ vortices. (d) represents a $p=-1$ vortex.

can be constructed by introducing complex numbers $z=x+iy$, $z_{mn}=x_{mn}+iy_{mn}$, and by using the prescription

$$\Phi(\vec{r})=\mathrm{Im}\sum_{m,n}\log(z-z_{mn})\ ,$$

but this series is not well behaved for an unbounded array. An alternative and rigorous procedure shows that $\Phi(\vec{r})$ satisfies certain quasiperiodic relations. For the case of a square lattice with basis vectors $\vec{b}_1=b\hat{x}$ and $\vec{b}_2=b\hat{y}$, $\Phi(\vec{r})$ obeys the recursion relation

$$\Phi(\vec{r}+m\vec{b}_1+n\vec{b}_2)=\Phi(\vec{r})+\pi b^{-1}(my-nx)\pm\pi(m+n+mn)\ , \quad (9)$$

where the choice of sign is unimportant because Φ is defined only modulo 2π. Furthermore, the lattice rotates about some lattice site (the origin) and $\Phi(\vec{r})$ inside the first square unit cell ($|x|<\frac{1}{2}b$, $|y|<\frac{1}{2}b$) has the rapidly converging expansion

$$\Phi(\vec{r})\approx\phi-\frac{1}{15}\left[\frac{1.854r}{b}\right]^4\sin4\phi-\frac{2}{525}\left[\frac{1.854r}{b}\right]^8\sin8\phi+\cdots\ . \quad (10)$$

It is then straightforward to evaluate Φ throughout the array, with the result shown in Fig. 2. A similar analysis is possible for a triangular array, but it is unnecessary for our purposes.

It is evident by inspection that $\Phi(\vec{r})$ is not a periodic function (even modulo 2π). Instead, the phase twists increasingly rapidly in moving away from the origin. This behavior must reflect the presence of a net induced circulating superfluid velocity arising from the uniform density of vortices, since Eq. (1) implies that the change of phase between two points is just the corresponding line integral of $\vec{v}_s$. It also follows that $\vec{v}_s=\vec{\nabla}\Phi$ cannot be periodic. Indeed, the lattice itself executes solid-body rotation, i.e., it is stationary in a frame rotating with the angular speed given by Eq. (8), where p is the circulation per unit cell of area A_c (here $N_c=1$). Consequently, we infer that the quantity

$$\vec{v}_s-\vec{v}_n=\vec{\nabla}\Phi-(\pi p/A_c)\hat{z}\times\vec{r} \quad (11)$$

is strictly periodic, and this relation holds for general two-dimensional vortex lattices.

In the rotating frame, it follows that the relevant part of the free-energy density $\tilde{f}=\frac{1}{2}\rho_s(\vec{v}_s-\vec{v}_n)^2$ is periodic with the lattice symmetry, so that the total free energy can be found from that for a single unit cell. For simplicity, we introduce an equivalent circular Wigner-Seitz (WS) cell of area A_c/N_c given by Eq. (8) and radius

$$a=(p\hbar/m_4\Omega)^{1/2}\ , \quad (12)$$

which for $\Omega=1$ rad/sec is $a\approx0.01$ cm. Inside this cell, the true relative velocity is replaced by the axisymmetric flow $\vec{v}_s-\vec{v}_n=v\hat{\phi}$, where

$$v=p/r-m_4\Omega r/\hbar=p(r^{-1}-r/a^2)\ . \quad (13)$$

Note that $v=0$ on the boundary of the circular WS cell, although this relation is not generally correct for the true polygonal unit cell. An elementary integration now gives the approximate free energy per unit cell

$$\tilde{F}\equiv\int_{\mathrm{cell}}d^2r\,\tilde{f}=\pi\rho_s p^2[\ln(a/\xi)-\tfrac{3}{4})]\ , \quad (14)$$

omitting small terms of order $(\xi/a)^2$. Detailed calculations[11] show that Eq. (14) differs from the exact value for the square or triangular lattices by only a small correction.

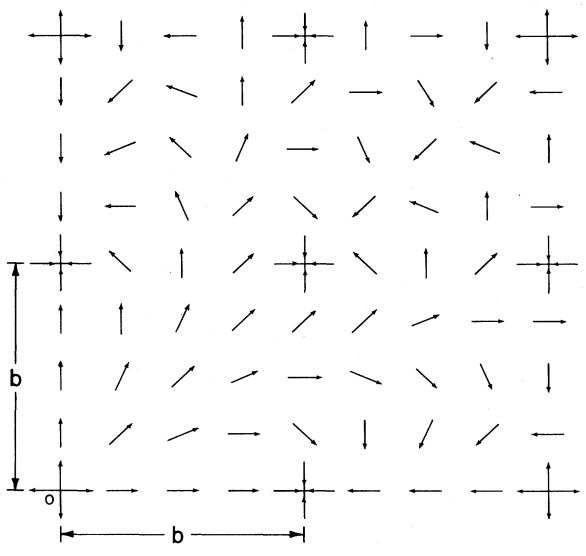

FIG. 2. Phase-angle representation of the function $\Phi(\vec{r})$ for a square lattice of vortices. Vectors twist increasingly rapidly in moving away from the center of rotation at 0.

B. Vortices in superfluid ^{3}He-A

In the case of superfluid ^{3}He, the spin-triplet p-wave order parameter $A_{\mu i}$ is a vector in spin space with respect to index μ and a vector in orbital space with respect to index i. For ^{3}He-A, it has the specific form[12]

$$A_{\mu i}=\Delta\hat{d}_\mu(\hat{\Delta}_1+i\hat{\Delta}_2)_i\ , \quad (15)$$

where $\hat{\Delta}_1$, $\hat{\Delta}_2$, and $\hat{l}\equiv\hat{\Delta}_1\times\hat{\Delta}_2$ are orthogonal unit vectors, and $\hat{l}$ is the direction of the orbital angular momentum of a Cooper pair. Thus, the orbital part of the order parameter is fixed by specifying the orientation of an orthonormal triad $(\hat{\Delta}_1,\hat{\Delta}_2,\hat{l})$ throughout space. A convenient way to parametrize the triad is to use the Euler angles (α,β,γ).[13] In this convention, α and β are the azimuthal and polar angles of the vector $\hat{l}$ with respect to some fixed set of axes $(\hat{x},\hat{y},\hat{z})$, and γ then represents an additional rotation about $\hat{l}$. Specifically, the auxiliary triad

$$\begin{aligned}\hat{l}&=(\hat{x}\cos\alpha+\hat{y}\sin\alpha)\sin\beta+\hat{z}\cos\beta\ ,\\ \hat{m}&=(\hat{x}\cos\alpha+\hat{y}\sin\alpha)\cos\beta-\hat{z}\sin\beta\ ,\\ \hat{n}&=-\hat{x}\sin\alpha+\hat{y}\cos\alpha\ ,\end{aligned} \quad (16a)$$

allows us to write the order parameter as

$$\hat{\Delta}_1+i\hat{\Delta}_2=e^{-i\gamma}(\hat{m}+i\hat{n}) . \tag{16b}$$

In ^{4}He, the physical properties are invariant under an overall constant rotation of the phase S, but local changes δS in phase between $\vec{r}$ and $\vec{r}+\delta\vec{r}$ are related to the superfluid velocity by $\delta S=\vec{v}_s\cdot\delta\vec{r}$. Similarly in ^{3}He-$A$, the change in the orbital part of the order parameter between $\vec{r}$ and $\vec{r}+\delta\vec{r}$ represents an infinitesimal rotation $\delta\vec{\omega}$ of the rigid triad. Part of this rotation is a change in the local direction of $\hat{l}$, and the remainder $\delta\vec{\omega}\cdot\hat{l}$ is a rotation about the direction $\hat{l}$. It is this last part that is analogous to the local phase change in ^{4}He. The corresponding superfluid velocity in ^{3}He-A has the form

$$\vec{v}_s=-\vec{\nabla}\gamma-\cos\beta\vec{\nabla}\alpha . \tag{17}$$

This relation is the appropriate generalization of Eq. (1) for ^{3}He-A and has several important features.

(i) $\mathrm{curl}\vec{v}_s$ does not, in general, vanish. Instead,

$$\mathrm{curl}\vec{v}_s=\sin\beta(\vec{\nabla}\beta\times\vec{\nabla}\alpha) , \tag{18}$$

which shows, in the absence of singularities of γ, that the superfluid vorticity is determined by $\hat{l}$ and its derivatives.[5]

(ii) This distributed vorticity means that there is no quantization of circulation in superfluid ^{3}He-A, although there may also be additional concentrated vorticity associated with the singularities of γ.

(iii) The hydrodynamic description of ^{3}He-A uses the vector fields $\vec{v}_s$ and $\hat{l}$. Since both follow directly from the three Euler angles, they are not independent variables. Indeed, Eq. (18) is often considered a constraint relating $\mathrm{curl}\vec{v}_s$ and $\hat{l}$.[5]

The Euler angle β may have values between 0 and π. In contrast, the angles α and γ can increase without limit; in this sense both are analogous to the phase function S for superfluid ^{4}He. Many of the interesting and unusual properties of superfluid ^{3}He-A follow from the occurrence of two such functions. For example, a line singularity in S represents a vortex in ^{4}He through Eq. (1). Correspondingly, line singularities in α or γ lead to vortices and singular textures in ^{3}He-A. There are several different possibilities.

(i) If α and β are constant, then $\hat{l}$ is constant and the resulting superfluid velocity is given by

$$\vec{v}_s=-\vec{\nabla}\gamma . \tag{19}$$

Thus any singularity in γ will result in a "phase" vortex, essentially the same as a vortex in ^{4}He. In this case, $-\gamma$ plays the role of the phase function S, and all the previous relations about quantized vortices hold here as well. In particular, if $\gamma=-p\phi+\gamma_0$, then we have a p-fold quantized vortex with a velocity field that diverges near the axis as in Eq. (4), leading to a singular vortex. Similar considerations apply if α and β vary smoothly throughout space, so long as $\hat{l}$ is nonsingular.

(ii) If γ is constant, then $\vec{v}_s=-\cos\beta\vec{\nabla}\alpha$. Thus line singularities in α typically generate a singular superflow, and the resulting vortex may be called an $\hat{l}$ vortex, since, in general, $\hat{l}$ has singular regions where its direction is not defined. The exception is when $\sin\beta=0$ at the singularities of α (so that $\hat{l}=\pm\hat{z}$), but $\vec{v}_s$ remains singular. Alternatively, we can make $\vec{v}_s$ finite if $\cos\beta\to0$ near the vortex center, but $\hat{l}$ is then singular. In either case, the free-energy density diverges at the vortex core unless some cutoff procedure is used. A simple example of this class of singular vortices is (in cylindrical polar coordinates r,ϕ,z)

$$\alpha=p\phi+\alpha_0 , \quad \beta=\beta(r) , \quad \gamma=\gamma_0 , \tag{20}$$

where $\beta(0)=\pi/2$ and $\beta(r)$ has a finite slope at $r=0$ and increases smoothly to π for large r. The resulting $\vec{v}_s=-(p\cos\beta/r)\hat{\phi}$ looks like a p-fold quantized vortex at infinity, but $\vec{v}_s$ is everywhere bounded. On the other hand, $\hat{l}$ near the origin has precisely the form shown in Fig. 1 (a $p=1$ disgyration).

(iii) Both α and γ may have singularities, and, in general, the resulting texture has singularities in both $\vec{v}_s$ and $\hat{l}$. In certain cases, however, these separate singularities in α and γ combine to cancel, leaving a nonsingular texture in which $\vec{v}_s$ and $\hat{l}$ are smooth and bounded throughout space. This possibility arises for the following reason: In the special cases that the Euler angle $\beta=0$, the rotations labeled by α and γ are equivalent, so that only the sum $\alpha+\gamma$ is relevant. This feature is evident in the superfluid velocity (17), which becomes $\vec{v}_s=-\vec{\nabla}(\alpha+\gamma)$ when $\beta=0$. If α and γ have opposing singularities (so that $\alpha+\gamma$ is everywhere continuous) and if $\beta=0$ in that region, the resulting superfluid velocity will be bounded and nonsingular there. For example, if $\alpha=\phi+\alpha_0$ (a $p=1$ singularity, as shown in Fig. 1) and $\beta(r)$ vanishes at $r=0$, then $\hat{l}$ varies smoothly in the vicinity of the origin with no singularity

$$\hat{l}=\sin\beta(\hat{r}\cos\alpha_0+\hat{\phi}\sin\alpha_0)+\hat{z}\cos\beta . \tag{21a}$$

In addition, taking $\gamma=-\phi$ (to make $\alpha+\gamma$ nonsingular), the superfluid velocity is purely azimuthal, with magnitude

$$v_s=(1-\cos\beta)/r . \tag{21b}$$

This quantity evidently vanishes as $r\to0$, if $1-\cos\beta\to0$ faster than r.

The asymptotic behavior of the superfluid velocity as $r\to\infty$ is also interesting. If $\beta(r)$ approaches $\pi/2$ for large r, the texture becomes planar with one unit of circulation at the boundary. This is the texture studied by MH for a cylinder.[5] Instead, if $\beta(r)$ approaches π for large r, then the texture has two units of circulation and is the coreless 4π vortex studied by AT.[3] More generally, the orbital part of the order parameter in Eq. (16b) can be written exactly as

$$\hat{\Delta}_1+i\hat{\Delta}_2=e^{-i(\alpha+\gamma)}(\hat{x}+i\hat{y})$$
$$-e^{-i\gamma}[(\hat{x}\cos\alpha+\hat{y}\sin\alpha)(1-\cos\beta)+\hat{z}\sin\beta] \tag{22}$$

showing that $\hat{\Delta}_1+i\hat{\Delta}_2$ is continuous across a region where $\cos\beta=1$ if $\alpha+\gamma$ is continuous there. This representation

also confirms that $\alpha+\gamma$ is the net rotation angle about $\hat{l}=\hat{z}$.

A similar argument applies to regions where $\cos\beta=-1$, in which case $\gamma-\alpha$ is the rotation about $\hat{l}=-\hat{z}$ and must be nonsingular. For the specific example $\alpha=-\phi+\alpha_0$ [a $p=-1$ singularity, as shown in Fig. 1(d)] and $\beta(0)=\pi$, the $\hat{l}$ texture is no longer axisymmetric, but it is again nonsingular,

$$\hat{l}=[\hat{r}\cos(2\phi-\alpha_0)-\hat{\phi}\sin(2\phi-\alpha_0)]\sin\beta+\hat{z}\cos\beta\ . \tag{23a}$$

The additional choice $\gamma=-\phi$ then gives a bounded superfluid velocity with purely azimuthal component

$$v_s=(1+\cos\beta)/r \tag{23b}$$

that is asymptotically a positive singly quantized vortex if $\cos\beta$ approaches 0 for large r. This texture is called the mixed-twist texture[14] because $\hat{l}$ rotates once about $\hat{z}$ in the negative sense on once encircling the origin (as in the $p=-1$ case of Fig. 1), in contrast to the positive rotation of $\hat{l}$ for the $p=+1$ texture in Eq. (21a). Nevertheless, the superfluid velocity for both $p=\pm1$ textures is in the $+\hat{\phi}$ direction.

It is interesting to consider how uniform normal-fluid rotation with angular velocity Ω affects the equilibrium configuration of superfluid ^{3}He-A. As in superfluid ^{4}He, the normal fluid executes solid-body rotation with $\vec{v}_n=2m_3\hbar^{-1}\vec{\Omega}\times\vec{r}$. In the rotating frame of reference the free-energy density $\tilde{f}$ is obtained from f for $\vec{\Omega}=0$ by replacing $\vec{v}_s$ everywhere by the relative velocity $\vec{v}_s-\vec{v}_n$, and subtracting the constant $\frac{1}{2}\rho v_n^2$ [compare Eq. (6)]. This prescription is easily implemented in the hydrodynamic model,[7] where Δ in Eq. (15) is assumed to be fixed and the only spatial variations arise from the reorientation of the unit vectors $\hat{d}$, $\hat{\Delta}_1$, and $\hat{\Delta}_2$; this model is particularly useful in studying nonsingular textures, where the temperature dependence occurs only in the hydrodynamic parameters appearing in f.[15,16] However, the hydrodynamic model cannot be used for systematic studies of singular regions (for example, a vortex core), where the order parameter departs from its A-phase form in Eq. (15). In this case, we start with the more general Ginzburg-Landau (GL) free-energy density, which, however, holds only near the transition temperature.[17] The transformation of the GL free energy to rotating coordinates is straightforward; we replace the gradient operator $\vec{\nabla}$ in the bending energy [see Eq. (29) below] by $\vec{\nabla}-2m_3i\hbar^{-1}(\vec{\Omega}\times\vec{r}\,)$ (identically equal to $\vec{\nabla}-i\vec{v}_n$).

From our previous discussion we expect that bulk rotating superfluid ^{3}He-A will have an array of vortices or textures arranged in a regular lattice with a unit cell of area A_c.[4,18] The order parameter depends only on the two-dimensional coordinate $\vec{r}$. Furthermore, $\hat{l}$ and $\vec{v}_s-\vec{v}_n$ must have the periodicity of the lattice. In particular [see Eq. (16a)], $\alpha(\vec{r}\,)$ should be periodic modulo 2π. If, in addition, $\alpha(\vec{r}\,)$ is continuous, then the same arguments used in obtaining Eq. (11) imply that $\vec{\nabla}\alpha-(\pi p/A_c)\hat{z}\times\vec{r}$ is periodic, where p is the net winding number of α encircling the unit cell once. Evidently, the second term conflicts with the periodicity (modulo 2π) of α unless either $p=0$ or α is not continuous. In the following we consider these possibilities separately.

A texture with no net winding of α has been proposed independently by Ho[14] and by Fujita *et al.*,[4] in which $\alpha(\vec{r}\,)$ has $p=+1$ singularities at the corners of a square two-dimensional lattice and $p=-1$ singularities at the centers. The unit cell (shown dotted in Fig. 3) contains two singularities of each type which give a net circulation of α equal to zero. Furthermore, β varies smoothly from 0 at the $+1$ singularities in α (shown as circles in Fig. 3) to π at the -1 singularities (shown as $\times$'s in Fig. 3), so the $\hat{l}$ texture flares up at the positive singularities of α and down at the negative singularities. This up-down arrangement (the type-I structure of Fujita *et al.*) ensures that $\hat{l}$ has no singularities, and the resulting elastic contribution to the hydrodynamic free-energy density is finite everywhere. To ensure that $\vec{v}_s$ is also finite, it suffices to choose the remaining Euler angle γ to have -1 singularities at both sets of sites; the texture can then be viewed as a set of interpenetrating MH nonsingular vortices (the 0 sites) and mixed-twist nonsingular vortices (the $\times$ sites), arranged on two interlaced square lattices [see the discussion of Eqs. (21)—(23)]. As shown below, this nonsingular texture appears to have the lowest free energy for bulk ^{3}He-A in zero magnetic field at low and moderate angular velocity.

Another way to arrange vortices on a lattice is to give up the continuity of α. This is the situation for the structure suggested by Volovik and Kopnin,[18] and analyzed in detail by Fujita *et al.* (their type-II structure). In this case, one takes a two-dimensional triangular lattice and constructs the WS polygons enclosing each unit cell.[19] Let $\beta=0$ at the lattice sites ($\hat{l}$ is up) and $\beta=\pi$ along the boundary of the unit cell ($\hat{l}$ is down). If $\Phi(\vec{r}\,)$ is the phase function for singly quantized vortices [Eqs. (9) and (10)] arranged on the same lattice sites, then the choice $\alpha-\gamma=2\Phi$ ensures that the order parameter is continuous on the unit-cell boundaries [see the discussion before Eq. (23)]. However, $\alpha(\vec{r}\,)$ must be periodic (modulo 2π) and hence cannot be a multiple of Φ. Instead, we choose $\alpha(\vec{r}\,)=[\Phi(\vec{r}\,)]$, where the square bracket means the periodic repetition of Φ in the central unit cell throughout the entire lattice. For a square lattice, this function is

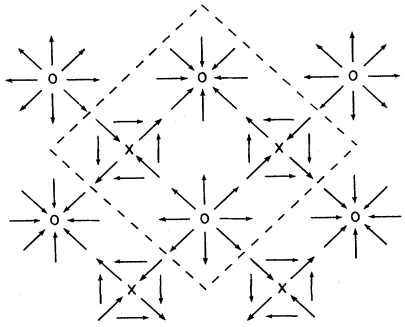

FIG. 3. Type-I lattice. Unit cell (dashed box) encloses two MH (0 sites) and two mixed-twist ($\times$ sites) vortex textures.

given explicitly in Eq. (10), and the generalization to other geometries is not difficult.[20] Note that this α is discontinuous at the cell boundaries, which permits it to remain periodic modulo 2π while avoiding the extra twist normally associated with the presence of all positive singularities. The texture looks locally like a coreless AT vortex in each unit cell. Although the $\hat{l}$ texture is continuous everywhere, certain derivatives of $\hat{l}$ (including $\mathrm{div}\hat{l}$ and $\mathrm{curl}\hat{l}$) are discontinuous on the cell boundaries, implying that $\hat{l}$ has singular surfaces analogous to higher-order vortex sheets. It is an open question whether these discontinuities affect the stability of the texture.

To study the corresponding superfluid velocity, it is helpful to rewrite Eq. (17) as

$$\vec{v}_s = -\vec{\nabla}(\gamma-\alpha)-(1+\cos\beta)\vec{\nabla}\alpha \ . \tag{24}$$

The first term is differentiable and continuous, but not periodic modulo 2π; it contains the overall induced rotation that makes the lattice stationary in the rotating frame. The second term of Eq. (24) is periodic and continuous but not differentiable on the cell boundary, again implying the presence of certain higher-order discontinuities, although the vorticity [Eq. (18)] vanishes identically on the cell boundaries. It follows from Eq. (24) that the superfluid velocity has a net circulation of 4π on once traversing the boundary of the unit cell, confirming the interpretation of this texture as an array of AT vortices. All estimates indicate that this configuration has a significantly higher free energy than that for the texture shown in Fig. 3.

Besides these lattices of nonsingular textures, ^{3}He-A may, in principle, rotate by forming an array of singular vortex textures similar to that of rotating ^{4}He. In ^{3}He-A the closest analog of the rotating ^{4}He vortex lattice is described by $\gamma=-\Phi(\vec{r})+\gamma_0$, with α, β, and γ_0 equal to constants. In this case $-\gamma$ plays the role of the phase function S for ^{4}He and describes a lattice of 2π phase vortices embedded in a uniform $\hat{l}$ texture. Since $\vec{v}_s=\vec{\nabla}\Phi(\vec{r})$ is singular and $\hat{l}$ is nonsingular, there is necessarily a core around each singularity of $\vec{v}_s$ where the order parameter deviates from the local A-phase form. These singular phase vortices are important in ^{3}He-A at high rotational speed.

Muzikar's analysis[21] of the structure of a DeGennes disgyration suggests that a lattice of more complicated singular vortex textures may be the equilibrium configuration of rotating ^{3}He-A. An axisymmetric vortex with 2π circulation of the type studied by Muzikar has the form

$$A_{\mu i}=\Delta\hat{z}_\mu[\cos\beta(\cos\alpha_0\hat{r}_i+\sin\alpha_0\hat{\phi}_i)-\sin\beta\hat{z}_i +i(-\sin\alpha_0\hat{r}_i+\cos\alpha_0\hat{\phi}_i)] \tag{25}$$

with $\pi/2<\beta<\pi$, $\alpha=\alpha_0+\phi$, and $\gamma=0$. The corresponding texture and superfluid velocity from Eqs. (16a) and (17) are

$$\vec{v}_s=-\cos\beta\frac{\hat{\phi}}{r} \ , \tag{26}$$

$$\hat{l}=\sin\beta(\cos\alpha_0\hat{r}+\sin\alpha_0\hat{\phi})+\cos\beta\hat{z} \ . \tag{27}$$

Thus for $\beta\to\pi$ at large distances the order parameter describes a singly quantized vortex $\hat{l}=-\hat{z}$. At short distances $\beta\to\pi/2$ and the velocity field is nonsingular, but the texture $\hat{l}\to\cos\alpha_0\hat{r}+\sin\alpha_0\hat{\phi}$ is singular. Energy considerations (see Sec. III) show that the radial dipole-unlocked disgyration ($\alpha_0=0$, $\beta=\pi/2$) is favored for distances less than $O(L_D)$. But since $\hat{l}$ is still singular, there is necessarily a core with radius $r_c\sim\xi$ where the order parameter deviates from the A-phase form. Muzikar showed that the polar core gives a lower energy than either the normal core ($\Delta\to0$) or the planar core. In particular the axisymmetric order parameter

$$A_{\mu i}=\sqrt{2}\Delta\hat{z}_\mu(-\cos\theta\hat{z}_i+i\sin\theta\hat{\phi}_i) \tag{28}$$

interpolates between the dipole-unlocked radial disgyration for $\theta=\pi/4$ and the polar phase for $\theta=0$.

We construct a lattice of singular vortex textures that have the same local structure as that described by Eqs. (25) and (28) by choosing $\alpha=[\Phi(\vec{r})]$ and $\gamma=[\Phi(r)]-\Phi(\vec{r})$ with β periodic, continuous, and varying between π on the cell boundary and $\pi/2$ on a closed contour in the cell interior with a radial dimension of order ξ. Inside this contour the order parameter changes continuously from a $p=1$ singularity in $\hat{l}$ [Fig. 1(a)] to the polar phase at the center of the cell. As with the type-II nonsingular structure of Ref. 4, α is periodic but not continuous across the cell boundary. Thus, although both $\hat{l}$ and $\vec{v}_s$ are continuous, neither is differentiable on the cell boundary. It is also unknown whether the singular surfaces that result from derivatives of $\hat{l}$ and $\vec{v}_s$ affect the stability of this lattice of 2π vortex textures.

III. FREE ENERGY OF VORTEX TEXTURES IN ROTATING ^{3}He-A

In this section we examine the energy and relative stability of the various structures discussed in Sec. II as possible equilibrium states for rotating ^{3}He-A in zero magnetic field. At low and moderate rotational speeds (but still $\Omega\gg\Omega_{c1}$) the nonsingular lattice of interpenetrating MH and mixed-twist textures (we shall use the notation of Ref. 4 and refer to this lattice as the type-I structure) has the lowest energy. There is a textural transition to a lattice of singular 2π vortex textures with $\hat{l}=-\hat{z}$ on each cell boundary at a rotation speed of $\Omega_1\simeq\hbar/2m_3(3L_D)^{-2}\approx32$ rad/sec for $T\simeq T_c$. The structure of these vortex textures (which we call $\hat{z}$ vortices from here on) varies from a 2π vortex to dipole-unlocked radial disgyration to polar core within each cell [see Eqs. (25)–(28)]. There is a second textural transition at a much higher rotational speed $\Omega_2\approx10^{-1}\Omega_{c2}$ to a lattice of singular 2π vortices with normal cores and $\hat{l}$ uniform and perpendicular to the rotation axis [see the paragraph above Eq. (25)]. We call these vortices $\hat{x}$ vortices. This lattice is consistent with Schopohl's result[8] that for very high rotational speeds ($\Omega\approx\Omega_{c2}$) the equilibrium state of rotating ^{3}He-A is a lattice of singular vortices with normal cores. The rest of this section discusses the calculations that lead to these conclusions.

The equilibrium configuration of ^{3}He-A in a rotating container is determined by minimizing the free-energy functional in the rotating frame. For temperatures $T \lesssim T_c$ this functional is given by the GL free energy[6]

$$\tilde{F} = \int d^3r \{ f_u[A] + f_D[A] + f_g[(\vec{\nabla} - i\vec{v}_n)A] \} , \tag{29a}$$

$$f_u[A] = \alpha \mathrm{Tr}(AA^\dagger) + \beta_1 |\mathrm{Tr}(A\tilde{A})|^2 + \beta_2 [\mathrm{Tr}(AA^\dagger)]^2 + \beta_3 \mathrm{Tr}[A\tilde{A}(A\tilde{A})^*] + \beta_4 \mathrm{Tr}[(AA^\dagger)^2] + \beta_5 \mathrm{Tr}[AA^\dagger(AA^\dagger)^*] , \tag{29b}$$

$$f_D[A] = g_D \{ |\mathrm{Tr}A|^2 + \mathrm{Tr}(AA^*) - \tfrac{2}{3}\mathrm{Tr}(AA^\dagger) \} , \tag{29c}$$

$$f_g[\vec{\nabla}A] = K_1(\nabla_a A_{ba})(\nabla_c A^*_{bc}) + K_2(\nabla_a A_{bc})(\nabla_a A^*_{bc}) + K_3(\nabla_a A_{bc})(\nabla_c A^*_{ba}) , \tag{29d}$$

where f_u is the uniform free-energy density that determines the condensation energy, f_D is the dipole energy, and $f_g[\vec{\nabla}A]$ is the second-order gradient energy.

For the uniform equilibrium A phase, the order parameter is given by Eq. (15) with $\Delta^2 = |\alpha|/4\beta_{245}$ and $|\hat{l}\cdot\hat{d}| = 1$ which minimizes the dipole energy in Eq. (29c). The parameter Δ defined by Eq. (15) and (29b) corresponds to the maximum value of the anisotropic A-phase energy gap. For slowly varying textures in ^{3}He-A, the order parameter is of the A-phase form [Eq. (15)] with the orientation of the triad $(\hat{\Delta}_1, \hat{\Delta}_2, \hat{l})$ and $\hat{d}$ varying smoothly in space. For the dipole-unlocked A phase the free-energy density, measured relative to the uniform equilibrium free-energy density for dipole-locked ^{3}He-A, reduces to the hydrodynamic form

$$f = \tfrac{1}{2}\rho_s v_s^2 - \tfrac{1}{2}\rho_0(\hat{l}\cdot\vec{v}_s)^2 + C\vec{v}_s\cdot(\vec{\nabla}\times\hat{l}) - C_0(\vec{v}_s\cdot\hat{l})[\hat{l}\cdot(\vec{\nabla}\times\hat{l})] + \tfrac{1}{2}K_s(\vec{\nabla}\cdot\hat{l})^2 + \tfrac{1}{2}K_t[\hat{l}\cdot(\vec{\nabla}\times\hat{l})]^2 + \tfrac{1}{2}K_b|\hat{l}\times(\vec{\nabla}\times\hat{l})|^2 + \tfrac{1}{2}K_4\vec{\nabla}\cdot[\hat{l}(\vec{\nabla}\cdot\hat{l}) - (\hat{l}\cdot\vec{\nabla})\hat{l}] + \tfrac{1}{2}K_5(\hat{l}\cdot\vec{\nabla}d_a)^2 + \tfrac{1}{2}K_6[(\hat{l}\times\vec{\nabla})_a d_b]^2 + \tfrac{1}{2}\rho_{||}L_D^{-2}[1-(\hat{l}\cdot\hat{d})^2] . \tag{30a}$$

The hydrodynamic free-energy density defined by Eq. (30a) is not restricted to T near T_c; however, the parameters in Eq. (30a) are related to the GL coefficients in this limit (see Appendix). In the calculations described below we use the temperature-dependent hydrodynamic parameters calculated by Williams[22] in the weak-coupling Bardeen-Cooper-Schrieffer (BCS) plus Fermi-liquid theory. For $T \simeq T_c$ the weak-coupling BCS theory predicts $K_1 = K_2 = K_3 \equiv K = \frac{1}{5}N(0)\xi_0^2$, where $\xi_0 \simeq 0.13\hbar v_F/k_B T_c \approx 120$ Å is related to the temperature-dependent coherence length

$$\xi(T) \equiv (K/|\alpha|)^{1/2} = [\tfrac{5}{3}(1 - T/T_c)]^{-1/2}\xi_0 ,$$

$\alpha = \frac{1}{3}N(0)(T - T_c)/T_c$, and $N(0)$ is the density of states for one spin population. The other length scale that enters is the dipole length $L_D = [K/g_D]^{1/2} \approx 6 \times 10^{-4}$ cm.

For spatial variations of the order parameter that occur on length scales which are large compared to L_D, the order parameter remains dipole locked. In this case, the free energy reduces to

$$f = \tfrac{1}{2}\rho_s v_s^2 - \tfrac{1}{2}\rho_0(\hat{l}\cdot\vec{v}_s)^2 + C\vec{v}_s\cdot(\vec{\nabla}\times\hat{l}) - C_0(\hat{l}\cdot\vec{v}_s)\hat{l}\cdot(\vec{\nabla}\times\hat{l}) + \tfrac{1}{2}K_s'(\vec{\nabla}\cdot\hat{l})^2 + \tfrac{1}{2}K_t'[\hat{l}\cdot(\vec{\nabla}\times\hat{l})]^2 + \tfrac{1}{2}K_b'|\hat{l}\times(\vec{\nabla}\times\hat{l})|^2 + \tfrac{1}{2}K_4'\vec{\nabla}\cdot[\hat{l}(\vec{\nabla}\cdot\hat{l}) - (\hat{l}\cdot\vec{\nabla})\hat{l}] , \tag{30b}$$

where the dipole-locked parameters are related to the dipole-unlocked parameters by Eqs. (A1) in the Appendix.

The coupling of the superfluid to the uniform rotation of the container and normal fluid is made by the transformation $\vec{\nabla}\overleftrightarrow{A} \to (\vec{\nabla} - i\vec{v}_n)\overleftrightarrow{A}$ in Eq. (29d) and $\vec{v}_s \to \vec{v}_s - \vec{v}_n$ in Eqs. (30). For fast rotating ^{3}He-A ($\Omega_{c1} \ll \Omega \ll \Omega_{c2}$), $\tilde{F}$ is minimized by a lattice of vortex filaments which mimic rigid-body rotation far from the center of rotation. The relation between the cell area and the rotation speed, in analogy to Eq. (8) for ^{4}He, is

$$A_{\mathrm{cell}} = \frac{p\pi\hbar}{2m_3\Omega} , \tag{31}$$

where p is the number of circulation quanta per cell.

To estimate the relative energies of different vortex-texture lattices we note that the free-energy density is periodic so that $\tilde{F} = \sum_{\mathrm{cells}} \tilde{F}_{\mathrm{cell}}$ where $\tilde{F}_{\mathrm{cell}}$ is the free energy of the unit cell. We use a WS approximation to calculate $\tilde{F}_{\mathrm{cell}}$. The equivalent WS area is given by Eq. (31) and radius

$$a = (p\hbar/2m_3\Omega)^{1/2} . \tag{32}$$

If the texture $\hat{l}(\vec{r})$ has the same axial symmetry of the cell, then for a first approximation the true relative velocity is replaced by the axisymmetric flow $\vec{v}_s - \vec{v}_n = v(r)\hat{\phi}$. We expect the WS approximation to be reasonably good for estimating the relative energies of arrays of vortex textures with different structure provided $a \gg \xi$ ($\Omega \ll \Omega_{c2}$). However, the WS approximation is clearly inadequate for determining the relative energies of different lattice geometries of the same type of vortex texture.

The single-cell WS approximation must also be used with care. For example, the term proportional to K_4 in Eq. (30a) gives a contribution to $\tilde{F}$ only at the surface of the container. This surface term is the same for all lattice geometries because $\hat{l}$ is normal to the container wall. However, if Eq. (30a) is used to calculate $\tilde{F}_{\rm cell}$ then there is a contribution from the K_4 term at the cell boundary. For the actual lattice these surface terms cancel because the surface normals on adjacent cell boundaries are in opposite directions. Thus, the K_4 term is not included in the estimates of $\tilde{F}_{\rm cell}$ using the WS approximation. Similarly, the coupling energy proportional to $\vec{v}\cdot(\vec{\nabla}\times\hat{l})$, with $\vec{v}=\vec{v}_s-\vec{v}_n$ being the flow field in the rotating frame, also contains spurious surface contributions to $\tilde{F}_{\rm cell}$. This is easily seen by using vector identities and the MH relation for $\vec{\nabla}\times\vec{v}_s$ to write

$$\vec{v}\cdot(\vec{\nabla}\times\hat{l})=-\hat{l}\cdot(\vec{\nabla}\times\vec{v}_n)+\tfrac{1}{2}\vec{\nabla}\cdot\{[\hat{l}(\vec{\nabla}\cdot\hat{l})-(\hat{l}\cdot\vec{\nabla})\hat{l}]-2(\vec{v}\times\hat{l})\}\ .$$

Thus the hydrodynamic free energy that we use to calculate $\tilde{F}_{\rm cell}$ for dipole-locked textures is

$$\tilde{f}=\tfrac{1}{2}\rho_s v^2-\tfrac{1}{2}\rho_0(\hat{l}\cdot\vec{v})^2-C\hat{l}\cdot(\vec{\nabla}\times\vec{v}_n)-C_0(\vec{v}\cdot\hat{l})(\hat{l}\cdot\vec{\nabla}\times\hat{l})+\tfrac{1}{2}K_s'(\vec{\nabla}\cdot\hat{l})^2+\tfrac{1}{2}K_t'(\hat{l}\cdot\vec{\nabla}\times\hat{l})^2+\tfrac{1}{2}K_b'|\hat{l}\times(\vec{\nabla}\times\hat{l})|^2\ . \tag{33}$$

Although the spurious surface terms are obvious from Eqs. (30), they are easily overlooked if $\tilde{F}_{\rm cell}$ is calculated directly from the GL functional in Eqs. (29).

A. Nonsingular vortex textures

The MH (or 2π) and AT (or 4π) structures in a cylindrical WS cell are defined by Eq. (21a) with $\beta(0)=0$, $\beta(a)=p\pi/2$, and $p=1(2)$ for the MH (AT) structure, and have velocity fields given by

$$\vec{v}=v(r)\hat{\phi}=\left[\frac{1-\cos\beta}{r}-\frac{pr}{a^2}\right]\hat{\phi}\ , \tag{34}$$

with $\vec{v}=0$ at both $r=0$ and a. The free energy per unit length calculated from Eq. (30b) with the trial function $\beta_{\rm trial}=p\pi r/2a$ is

$$\tilde{F}_{\rm cell}=\pi[0.0021\rho_s-0.9252C+(2.1910K_s'+0.8669K_b')\cos^2\alpha_0+(-0.0013\rho_0+2.5384K_t'+0.5194K_b'-0.1054C_0)\sin^2\alpha_0] \tag{35a}$$

for the MH structure, and

$$\tilde{F}_{\rm cell}=\pi[0.2672\rho_s+1.6211C+(3.6862K_s'+2.4674K_b')\cos^2\alpha_0+(-0.1952\rho_0-1.6035C_0+5.3241K_t'+0.8295K_b')\sin^2\alpha_0] \tag{35b}$$

for the AT structure. These equations indicate that there is very little conventional kinetic energy associated with these vortex textures. Furthermore, these energies depend on the local orientation of $\hat{l}$ through the rotation angle α_0. With the use of the weak-coupling hydrodynamic parameters, Eqs. (35) are minimized by a rotation of $\alpha_0=\pi/2$ for both textures; this is the conclusion of Fujita *et al.*[4] However, for general α_0 the supercurrent in the rotating frame with $\vec{v}$ given by Eq. (34),

$$\vec{j}_s=\rho_s\vec{v}-\rho_0(\hat{l}\cdot\vec{v})\hat{l}\ , \tag{36}$$

violates particle conservation. Therefore these textures cannot be solutions to the complete Euler-Lagrange equations obtained from Eq. (30b). The conclusion that $\alpha_0=\pi/2$ is therefore suspect because there may be textures with $\alpha_0\neq 0,\pi/2$ which satisfy particle conservation and have lower energy. This in fact is the case. For any given texture which violates particle conservation, we can construct a new texture which is topologically equivalent to the original and satisfies the conservation law. In particular, for either the MH or AT structure with energy $\tilde{F}_{\rm cell}$ we can add to $\vec{v}$ a nonsingular velocity field $\vec{v}_1\equiv-\vec{\nabla}\gamma_1$ with a corresponding current $\vec{j}_1$ such that $\vec{j}_s'\equiv\vec{j}_s+\vec{j}_1$ satisfies $\vec{\nabla}\cdot\vec{j}_s'=0$. The corresponding free energy is

$$\tilde{F}_{\rm cell}'=\tilde{F}_{\rm cell}-\int_S d\vec{S}\cdot\vec{j}_s'\gamma_1-\tfrac{1}{2}\int_{\rm cell}d^2r\,\vec{v}_1\cdot\vec{\vec{\rho}}_s\cdot\vec{v}_1\ . \tag{37}$$

If $\vec{j}_s'$ has no perpendicular component at the wall, then the surface term vanishes and the free energy is necessarily lowered by imposing the conservation law. For cylindrically symmetric MH and AT structures we can take γ_1 to be a function only of r, and find

$$\vec{v}_1=\sin\alpha_0\cos\alpha_0\sin\beta\times\frac{\{\rho_0\sin\beta v(r)+C_0[d\beta/dr+(1/r)\sin\beta\cos\beta]\}}{(\rho_s-\rho_0\sin^2\beta\cos^2\alpha_0)}\hat{r}\ . \tag{38}$$

The free-energy density for both structures is reduced by

$$\tilde{f}'-\tilde{f}=-\tfrac{1}{2}\vec{v}_1\cdot\vec{\vec{\rho}}_s\cdot\vec{v}_1=-\tfrac{1}{2}\sin^2\beta\sin^2\alpha_0\cos^2\alpha_0\times\frac{\{\rho_0\sin\beta v(r)+C_0[d\beta/dr+(1/r)\sin\beta\cos\beta]\}^2}{(\rho_s-\rho_0\sin^2\beta\cos^2\alpha_0)}\ , \tag{39a}$$

which vanishes for $\alpha_0=0,\pi/2$, but is strictly negative for other values of α_0. The reduction in energy $\delta\tilde{F}_{\rm cell}$

$=\int_{\text{cell}} d^2r(\tilde{f}'-\tilde{f})$ calculated with β_{trial} gives a minimum energy for $\alpha_0 \approx \pi/4$. To an excellent approximation $\delta\tilde{F}_{\text{cell}}$ for the MH texture is given by

$$\delta\tilde{F}_{\text{cell}}^{\text{MH}} = -\pi \sin^2(2\alpha_0)(4\rho_s)^{-1} \times (0.0010\rho_0^2 + 1.4830C_0^2 + 0.0720\rho_0 C_0) , \tag{39b}$$

and is also a small correction to the total MH energy, $|\delta\tilde{F}^{\text{MH}}|/\tilde{F}^{\text{MH}} \approx 0.03$ for $T \approx T_c$, but becomes significant at low temperatures, $|\delta\tilde{F}^{\text{MH}}|/\tilde{F}^{\text{MH}} \approx 0.5$ for $T \to 0$.

Since a lattice of only MH structures is not possible we must also consider the mixed-twist textures. The simplest 2π mixed-twist texture differs from the cylindrically symmetric MH texture by $\alpha(\phi) \to \alpha(-\phi) = -\phi + \alpha_0$; consequently, the mixed-twist texture [Eq. (23a)] is not axisymmetric. In a WS cell the mixed-twist structure with 2π circulation has a velocity field $\vec{v}' = \vec{v} + \vec{v}_1$ where

$$\vec{v} = [r^{-1}(1+\cos\beta) - r/a^2]\hat{\phi} , \tag{40a}$$

$$\vec{v}_1 = -\vec{\nabla}\gamma_1 , \tag{40b}$$

and $\vec{v}_1$ has zero circulation and is chosen to ensure particle conservation. The free energy of a 2π mixed-twist (mt) structure, neglecting $\vec{v}_1$, calculated using $\beta_{\text{trial}} = \pi - \pi r/2a$, is

$$\tilde{F}_{\text{cell}}^{\text{mt}} = \pi[0.0021\rho_s - 0.0007\rho_0 + 0.9253C + 0.0219C_0 + 0.0955K_s' + 0.2692K_t' + 0.6931K_b'] , \tag{41}$$

independent of α_0, and has significantly lower bending energy than the MH texture. This mixed-twist structure violates particle conservation because $\hat{l}(\vec{r})$ is not cylindrically symmetric. Imposing particle conservation lowers the energy of the mixed-twist structure by a small constant, also independent of α_0. Thus in the type-I lattice with both MH and mixed-twist structures interlaced there is no competition between the MH structures which prefer rotations of $\alpha_0 \approx \pi/4$ and mixed-twist structures whose energy is independent of α_0. Unlike the cylindrically symmetric MH and AT structures, γ_1 for the mixed-twist structure satisfies a complicated partial differential equation and cannot be taken as a function only of r. As an estimate of the energy of the type-I structure we add the energies of the MH texture calculated from Eqs. (35a) and (39b) with the mixed-twist energy calculated from Eq. (41); we neglect the $\vec{v}_1$ contribution to the mixed-twist energy which we expect to be small as it is for the MH structure. Similarly, we estimate the energy of the type-II structure by the energy of the 4π AT texture calculated from Eqs. (35b) and (39a). The dimensionless quantity $\tilde{F}_{\text{cell}}/\pi\rho_{||}$ for a type-I cell varies from 10 at $T/T_c = 1.0$ to approximately 6.5 at $T/T_c = 0.7$. The corresponding values for the type-II cell are approximately 1.4 times larger. Thus we find, in agreement with Fujita *et al.*, that the type-II lattice of AT vortex textures is never the minimum-energy state of rotating ^{3}He-A.

The estimates of the energy for these nonsingular vortex textures in cylindrical cells made with the linear trial function are generally good. Only minor improvements on these can be made by solving the Euler-Lagrange equations for $\beta(r)$ numerically. For example, we find that $|(F^{\text{MH}} - F_{\text{trial}}^{\text{MH}})/F_{\text{trial}}^{\text{MH}}| < 0.02$ for the MH structure with $\alpha_0 = 0$.

B. Singular vortex textures

At sufficiently high rotational speeds a lattice of singular vortex textures is energetically favored over the type-I lattice. The $\hat{z}$ vortices described by Eqs. (25)—(28) are good candidates for the equilibrium lattice of rotating ^{3}He-A at moderately high rotational speeds because the velocity field is nonsingular and the associated kinetic energy is low. The structure of the $\hat{z}$ vortex is determined by competition between the kinetic energy, bending energies, and dipole energy. The texture $\hat{l}(\vec{r})$ is dipole locked along $-\hat{z}$ at distances $a \geq r \gg L_D$, so in this outer region all of the energy is conventional kinetic energy. For distances $r \sim L_D$ the kinetic energy is comparable to the energy required to decouple $\hat{l}$ and $\hat{d}$. The 2π vortex with $\hat{l} = -\hat{z}$ is topologically equivalent to the dipole-unlocked disgyration, and since this texture can have smaller gradient energy than the vortex, the order parameter will rotate continuously from the vortex to the disgyration for $r < r_1 \sim L_D$. The superfluid velocity [Eq. (26)] vanishes inside the dipole radius where $\beta \to \pi/2$ for $r \ll L_D$; however, the texture is singular, so for distances $r \leq r_c \sim \xi$ (inside the core) the order parameter deviates from the A-phase form in order to eliminate the divergent gradient energy due to $\hat{l}$.

We estimate the energy of a lattice of $\hat{z}$ vortices using the WS cell approximation and the trial function

$$\beta(r) = \begin{cases} \pi, & r_1 < r < a \\ (\pi/2)(1 + r/r_1), & r < r_1 \end{cases} \tag{42}$$

which interpolates smoothly between the 2π vortex with $\hat{l} = -\hat{z}$ on the cell boundary and the disgyration with $\hat{l} = (\cos\alpha_0\hat{r} + \sin\alpha_0\hat{\phi})$ for $r \to 0$. The length scale r_1 is a variational parameter, which is of order L_D. We also fix $\hat{d} = \hat{z}$ and make cylindrical approximations for the other Euler angles, $\alpha = \phi + \alpha_0$ and $\gamma = \gamma_1(r)$. The rotation angle α_0 determines the local orientation of $\hat{l}$, while $\gamma_1(r)$ is nonsingular and is chosen to guarantee particle conservation. In the absence of γ_1 integration of Eq. (30a) for $r > r_c$ yields the free energy of the $\hat{z}$ vortex outside the core

$$\tilde{F}_{\text{cell}}^{>} = \pi(\rho_s[\ln(a/r_1) + 0.0741 + 0.1894(r_1/a)^2] + 2C[1 - 0.1894(r_1/a)^2] - (K_4 + C) + 0.1487\rho_{||}(r_1/L_D)^2 + \cos^2\alpha_0\{K_s[\ln(r_1/r_c) - 0.9572] + 0.3669K_b\} + \sin^2\alpha_0\{\rho_0[-0.3047 + 0.1801(r_1/a)^2 - 0.0346(r_1/a)^4] + C_0[-0.3906 + 0.1988(r_1/a)^2] + 0.5384K_t + K_b[\ln(r_1/r_c) - 1.1288]\}) . \tag{43}$$

Evidently the $\hat{z}$-vortex free energy is minimized by $\alpha_0=0$ since $K_b > 3K_s$ at all temperatures and the logarithms $\ln(r_1/r_c)\sim\ln(L_D/\xi)\sim 6.5$, dominate the bending energies. However, there may be $\hat{z}$ vortices with $\alpha_0\neq 0$ and γ_1 chosen to ensure particle conservation which have lower energy than the $\alpha_0=0$ $\hat{z}$ vortex. The construction of γ_1 for the $\hat{z}$ vortex follows the same argument as that given for the MH and AT vortex textures, so that $\vec{v}_1$ is given by Eq. (38) with $v(r)=-[r^{-1}\cos\beta+r/a^2]$, and the reduction in the $\hat{z}$-vortex energy density is given by Eq. (39a), except that now $\pi/2\leq\beta\leq\pi$. The kinetic anisotropy energy in Eq. (39a), which is nonzero only when $\vec{v}_s$ is not parallel to an eigenvector of $\overleftrightarrow{\rho}_s$, is minimized by $\alpha_0=\pi/4$ and competes with the orientation $\alpha_0=0$ that is preferred by the bending energies.

An analytic calculation of the kinetic anisotropy energy is not possible in general. However, a useful estimate of the magnitude of this energy can be obtained in the limit $\rho_0 \ll \rho_s, C_0$, which is valid for $T\to 0$. In this case integration of Eq. (39a) using $\beta_{\rm trial}$ in Eq. (42) gives

$$\delta\tilde{F}^{z}_{\rm cell}=-0.0139\pi(C_0^2/\rho_s)\sin^2(2\alpha_0)\ . \tag{44}$$

The $\hat{z}$-vortex energy outside of the core, given by the sum of Eqs. (43) and (44), is minimized by $\alpha_0=0$; equivalently $\hat{l}\to\hat{r}$ for $r\to 0$. The reason the $\hat{z}$ vortex prefers $\alpha_0=0$ whereas the MH vortex texture preferred $\alpha_0=\pi/4$ is that in the latter case the terms proportional to $\cos^2\alpha_0$ and $\sin^2\alpha_0$ in the free energy are essentially identical and so the unperturbed MH energy is almost independent of α_0. Furthermore, the $\vec{v}_1$ correction to $\tilde{F}^{\rm MH}_{\rm cell}$ has a large negative coefficient. For the $\hat{z}$ vortex the opposite occurs; the bending coefficients that enter the $\cos^2\alpha_0$ and $\sin^2\alpha_0$ terms are significantly different because this vortex is dipole unlocked.

Minimizing $\tilde{F}^{>}_{\rm cell}$ with respect to r_1 gives

$$r_1^2[0.1894(\bar{\rho}_s-2\bar{C})a^{-2}+0.1487L_D^{-2}]=(\tfrac{1}{2})(\bar{\rho}_s-\bar{K}_s)\ , \tag{45}$$

for $r_1<a$. The bar over hydrodynamic parameters means normalized to $\rho_{||}$. In the limit of slow rotation ($a\ll L_D$) $r_1=2.25L_D$ for $T\approx T_c$, and decreases to $r_1=1.95L_D$ at higher speed when $a=r_1$. For higher rotational speeds $r_1=a$ (see Fig. 4).

To complete the calculation of the $\hat{z}$-vortex energy we must add the core energy to $\tilde{F}^{>}_{\rm cell}$. The core energy is estimated using the GL functional and the order parameter in Eq. (28). Both the gradient energy and the change in the condensation energy contribute to the energy density so that

$$\begin{aligned}\tilde{f}^{<}=2\Delta^2\{&K_2[(d\theta/dr)^2+r^{-2}\sin^2\theta]\\&-K_3(r^{-1}d\theta/dr)\sin 2\theta\\&+K_2(2\xi^2)^{-1}(\beta_{13}/\beta_{245})\cos^2(2\theta)\}\ .\end{aligned} \tag{46}$$

With the use of the trial function $\theta(r)=\pi r/4r_c$, the weak-coupling coefficients $K_1=K_2=K_3\equiv(\frac{1}{4})\rho_{||}/\Delta^2$, and $\beta_{13}/\beta_{245}=\frac{1}{2}$, the core energy becomes

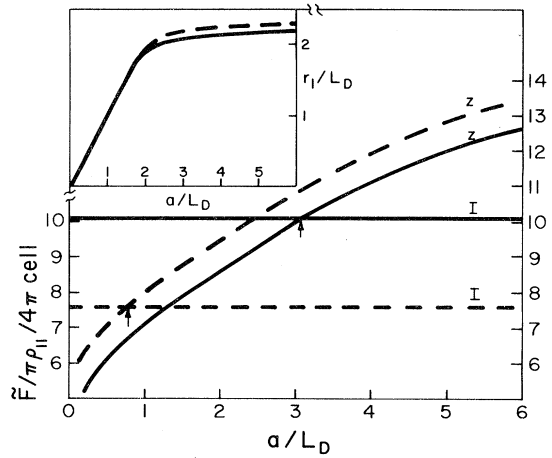

FIG. 4. Free energies for the type-I and $\hat{z}$ lattices are measured in units of $\pi\rho_{||}$ for a cell with two units (4π) of circulation. Arrows mark the WS cell radii at which textural transitions occur for $T/T_c=0.99$ (solid curves) and $T/T_c=0.8$ (dashed curves). Inset shows the dipole-core radius for the $\hat{z}$ vortices as a function of WS cell radius.

$$\tilde{F}^{<}_{\rm cell}=\pi\rho_{||}[0.0868+0.0372(r_c/\xi)^2]\ . \tag{47}$$

Thus the sum of Eqs. (43) and (47) for the total free energy for the $\hat{z}$ vortex becomes

$$\begin{aligned}\tilde{F}^{z}_{\rm cell}=\pi\{&\rho_s[\ln(a/r_1)+0.0741+0.1894(r_1/a)^2]\\&+2C[1-0.1894(r_1/a)^2]-(K_4+C)\\&+0.1487\rho_{||}(r_1/L_D)^2+K_s[\ln(r_1/r_c)-0.9572]\\&+0.3669K_b+\rho_{||}[0.0868+0.0372(r_c/\xi)^2]\}\ ,\end{aligned} \tag{48}$$

where $r_c=3.66\bar{K}_s^{1/2}\xi$ minimizes $\tilde{F}^{z}_{\rm cell}$. In Fig. 4 we show the free energies for the type-I and $\hat{z}$-vortex lattices as a function of a/L_D. For low rotational speeds (large a) the type-I lattice is favored at all temperatures. For $T/T_c=0.99$ there is a textural transition to a lattice of $\hat{z}$ vortices at $\Omega_1=(\hbar/2m_3)(3.0L_D)^{-2}\simeq 32$ rad/sec, and increases to $\Omega_1\simeq 4.5\times 10^2$ rad/sec at $T/T_c=0.8$, which is still small compared with $\Omega_{c2}\sim 10^7$ rad/sec.

For high rotational speeds essentially all of the $\hat{z}$-vortex energy is due to the bending of $\hat{l}$. In this limit a lattice of 2π-phase vortices with uniform $\hat{l}$, which has no bending energy,[23] has comparable energy to the $\hat{z}$-vortex lattice. Since $\hat{l}$ is the direction corresponding to the smallest eigenvalue of $\overleftrightarrow{\rho}_s$, the minimum-energy 2π vortex with uniform texture has $\hat{l}$ perpendicular to $\hat{z}$; we choose $\hat{l}=\hat{x}$. The free energy per unit cell of an $\hat{x}$-vortex lattice is calculated in analogy to that of the $\hat{z}$-vortex lattice. Outside the core ($r>r_c\sim\xi$) the free energy per unit length is all kinetic and given by

$$\tilde{F}^{>}_{\rm cell}=\int_{r>r_c} d^2r[\rho_s v^2-\rho_0(\hat{x}\cdot\vec{v})^2]/2\ , \tag{49}$$

where $\vec{v}=\vec{\nabla}\Phi(\vec{r})$. In the WS cell approximation $\vec{v}$ is replaced by the axial flow field[23]

$$\vec{v}=\left[r^{-1}\frac{(\bar{\rho}_s)^{1/2}}{1+\bar{\rho}_0\cos^2\phi}-\frac{r}{a^2}\right]\hat{\phi}\ , \tag{50}$$

which ensures particle conservation. The corresponding kinetic energy is

$$\tilde{F}^{>}_{\rm cell}=\pi\rho_{||}\{(\bar{\rho}_s)^{1/2}[\ln(a/r_c)-1]+\tfrac{1}{8}(1+\bar{\rho}_s)\}\ . \tag{51}$$

To estimate the $\hat{z}$-vortex core energy we take the core order parameter to be the $\hat{x}$-vortex order parameter for $r>r_c$ multiplied by the radial function $\delta(r)=r/r_c$. The free-energy density in the core is

$$\tilde{f}^{<}=\tfrac{1}{4}\rho_{||}\xi^{-2}(\delta^2-1)^2+\tfrac{1}{2}\rho_s[\delta^2 v^2+(\delta')^2] -\tfrac{1}{2}\rho_0[\delta^2(\hat{x}\cdot\vec{v})^2+(\hat{x}\cdot\vec{\nabla}\delta)^2]\ , \tag{52}$$

which, when integrated and combined with $\tilde{F}^{>}_{\rm cell}$, gives a total $\hat{x}$-vortex energy equal to

$$\tilde{F}^{x}_{\rm cell}=\pi\rho_{||}\{(\bar{\rho}_s)^{1/2}[\ln(a/\xi)-1.396-\tfrac{1}{4}\ln\bar{\rho}_s]+\tfrac{5}{8}(1+\bar{\rho}_s)\}\ , \tag{53}$$

and an optimum core radius $(r_c/\xi)^2=6(\bar{\rho}_s)^{1/2}$. Figure 5 shows the energies for the $\hat{x}$ and $\hat{z}$ vortices and the textural transition that occurs at $\Omega_2=0.10\Omega_{c2}$ $(a_2/\xi=6.3)$ for $T/T_c=0.8$. This transition to a lattice of singular vortices with normal cores is consistent with Schopohl's result[8] for $\Omega\approx\Omega_{c2}$.

IV. DISCUSSION

It is interesting to consider the formation of these vortex lattices. As seen in Fig. 6, the equilibrium texture in zero magnetic field depends on both the temperature and the angular velocity. If the system is cooled at rest into the A phase and then brought into rotation, the first structure formed should be the nonsingular type-I array, which will persist up to a relatively high angular velocity Ω_1 ($\approx$30 rad/sec). For still higher angular velocities, a lattice of singular $\hat{z}$ vortices has lower free energy, but the transition may be inhibited by a large energy barrier associated with the nucleation energy of the singular core regions and the rearrangement from square to triangular symmetry. In contrast, if normal ^{3}He is rotated and then cooled slowly into the A phase, the initial vortex array should be the singular $\hat{z}$ vortex with normal core,[8] followed by a transition at $\Omega_2(T)$ to the singular $\hat{z}$ vortex. In this case, the same energy barrier should help preserve the singular textures, even if the final T and Ω would favor the formation of a nonsingular type-I texture. Thus superfluid ^{3}He-A may display significantly more hysteresis than ^{4}He II because of the possibility of qualitatively different types of vortices.

An unambiguous detection scheme is essential for an experimental study of these equilibrium vortex lattices and their kinetics. Unfortunately, nuclear magnetic resonance (NMR) is not feasible as a probe of the nonsingular type-I lattice and the singular $\hat{z}$ lattice, because textural NMR analysis is difficult except in high fields, which suppress

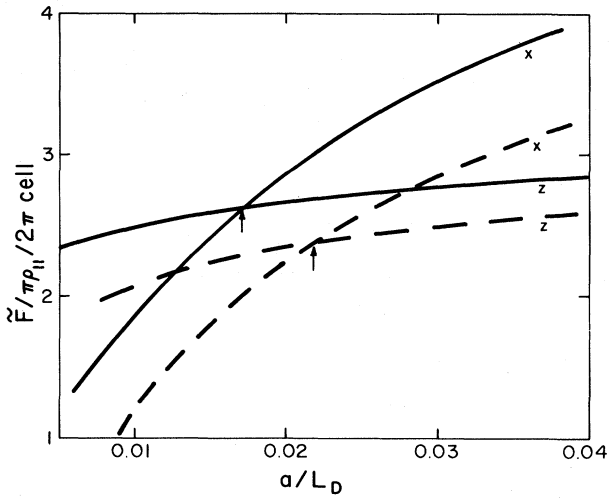

FIG. 5. Free energies for the $\hat{x}$ and $\hat{z}$ lattices are measured in units of $\pi\rho_{||}$ for a cell with 1 unit (2π) of circulation. Arrows mark the WS cell radii at which textural transitions occur for $T/T_c=0.6$ (solid curves) and $T/T_c=0.8$ (dashed curves).

both textures. Other possibilities are ions and zero sound. Here we concentrate on the ion-pulse shape as a way to measure the relative distribution of l_z^2 throughout the sample.[7] The basic observation is that the ionic mobility in ^{3}He-A is anisotropic; in an electric field $\vec{E}$, the resulting steady-state ion velocity is given by

$$\vec{v}=\mu\vec{E}-\mu_0\hat{l}(\hat{l}\cdot\vec{E})\ , \tag{54}$$

where $\mu_0/\mu\approx0.1$. Thus ions move faster in a region where $\hat{l}$ is perpendicular to $\vec{E}$. Consider the case of $\vec{E}$ along the rotation axis $(\hat{z})$, and assume that the ions move solely in the z direction, ignoring the small effect of focusing. In the presence of a texture $\hat{l}(\vec{r})$, an ion initially at $\vec{r}$ in the xy plane $(z=0)$ will arrive at the plane $z=L$ in a time

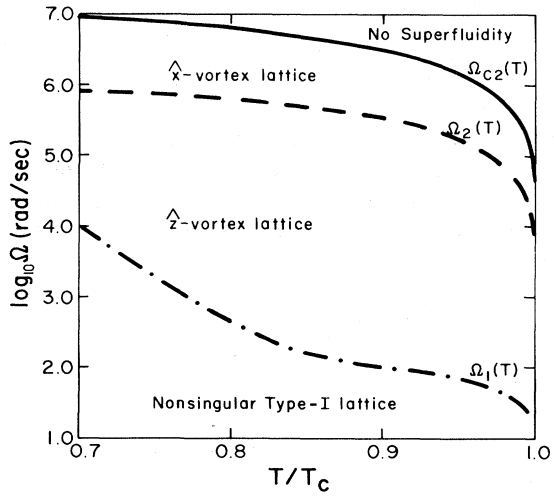

FIG. 6. Ω-T phase diagram for rotating ^{3}He-A in zero magnetic field.

$$t(\vec{r})=t_\perp[1-(\mu_0/\mu)l_z^2(\vec{r})]^{-1}\ , \tag{55}$$

where $t_\perp=L/\mu E$ is the arrival time for an ion moving perpendicular to $\hat{l}$. It is convenient to introduce the distribution function

$$P(x)=A_{\rm cell}^{-1}\int_{\rm cell}d^2r\,\delta(x-l_z^2(\vec{r}))\ . \tag{56}$$

Evidently, $P(x)dx$ is the probability that l_z^2 lies between x and $x+dx$, and $P(x)$ is normalized on the interval (0,1). For N ions initially distributed uniformly in the xy plane, the pulse shape at $z=L$ has the form

$$\frac{N(t)}{N}=\frac{\mu t_\perp}{\mu_0 t^2}P\left[\frac{\mu}{\mu_0}\frac{t-t_\perp}{t}\right]\ . \tag{57}$$

Consequently, the quantity $t^2N(t)$ provides a direct measure of $P(x)$.

In practice, the two relevant structures are the nonsingular type-I and the singular z lattices. For simplicity, we first consider the circular WS model for the type-I lattice with $\beta(r)=\pi r/2a$. The resulting integral is easily evaluated to give

$$P(x)=\frac{4}{\pi^2}\frac{\arccos x^{1/2}}{x^{1/2}(1-x)^{1/2}}\ , \tag{58a}$$

which diverges as $x\to 0$ and vanishes at $x=1$. The corresponding pulse (see Fig. 6 of Ref. 7) has a singular leading edge arising from the finite region (the cell boundary) where $\hat{l}$ is perpendicular to $\vec{E}$ (and hence large mobility); the negligible trailing edge comes from the central region where $\hat{l}$ is parallel to E, with a smaller mobility. A better approximation for the actual type-I lattice can be obtained with the periodic function

$$\cos\beta(x,y)=[\cos(2\pi x/b)+\cos(2\pi y/b)]/2\ ,$$

which has the proper linear behavior near the center of each cell (in contrast to that used in Ref. 4). The corresponding distribution function becomes

$$P(x)=\frac{2}{\pi^2 x^{1/2}}K[(1-x^2)^{1/2}]\ , \tag{58b}$$

where K is the complete elliptic integral. This function is very similar to that in (58a).

The other structure of interest is the z vortex, with l_z specified by Eq. (42). In the WS approximation, $\hat{l}$ is parallel to $\vec{E}$ throughout an annulus $r_1\le r\le a$ and becomes perpendicular to $\vec{E}$ only at the center. Thus the associated pulse should have a smooth leading edge and a singular trailing one, which is confirmed by the explicit expression

$$P(x)=\left[1-\frac{r_1^2}{a^2}\right]\delta(1-x)+\left[\frac{2r_1}{\pi a}\right]^2\frac{\arcsin x^{1/2}}{x^{1/2}(1-x)^{1/2}}\ . \tag{59}$$

It is apparent that these two lattice structures produce very different ion shapes.

The anisotropy of ultrasound attenuation may also be useful for identifying possible vortex lattices in rotating ^{3}He-A.[24] The A-phase sound attenuation depends on $\hat{q}\cdot\hat{l}=\cos\theta$, where $\hat{q}$ is the direction of sound propagation,[25,26]

$$\alpha=\alpha_{||}\cos^4\theta+2\alpha_c\sin^2\theta\cos^2\theta+\alpha_\perp\sin^4\theta\ . \tag{60}$$

The strong anisotropy observed[27] in α for ^{3}He-A is due to the rapid variations of α_c and $\alpha_\perp$ with temperature and frequency.[25,26]

Nakahara *et al.*[24] suggest that the magnetic field dependence of α can be used to identify the nonsingular type-I lattice. Since textures are typically distorted by fields greater than 20 G, these distortions will be reflected as changes in the sound attenuation with magnetic field through Eq. (60). Volovik and Hakonen propose that a lattice of singular vortices with $\hat{l}$ perpendicular to $\vec{\Omega}$ (e.g., the $\hat{x}$ vortex) could be identified by the anisotropy of α as a function $\hat{q}\cdot\hat{H}$ for both $\hat{q}$ and $\hat{H}$ perpendicular to $\vec{\Omega}$.

Here we note that because of the rapid variation of α_c and $\alpha_\perp$ near collective mode resonances, measurements of α in zero magnetic field (which would neither destabilize the type-I and z lattices nor distort the textures) may be used to differentiate between different vortex-texture lattices. In particular, for sound propagation along the rotation axis $\hat{q}=\hat{z}$ the effective attenuations obtained by averaging Eq. (60) over the WS cell for type-I, $\hat{z}$, and $\hat{x}$ vortex lattices are[28]

$$\begin{aligned}\alpha_I&=0.173\alpha_{||}+0.250\alpha_c+0.578\alpha_\perp\ ,\\ \alpha_z&=(1-r_1^2/a^2)\alpha_{||}+(r_1/a)^2\\ &\quad\times(0.578\alpha_{||}+0.250\alpha_c+0.173\alpha_\perp)\ ,\\ \alpha_x&=\alpha_\perp\ .\end{aligned} \tag{61}$$

The relatively large coefficient of $\alpha_\perp$ for the type-I lattice arises from the region near the cell boundary where $\hat{l}(\vec{r})$ is perpendicular to $\hat{q}$. The opposite is true for the $\hat{z}$ vortex; $\hat{l}$ is parallel to $\hat{q}$ in the outer region of each cell. Figure 7 shows the effective attenuation for the type-I, $\hat{z}$-,

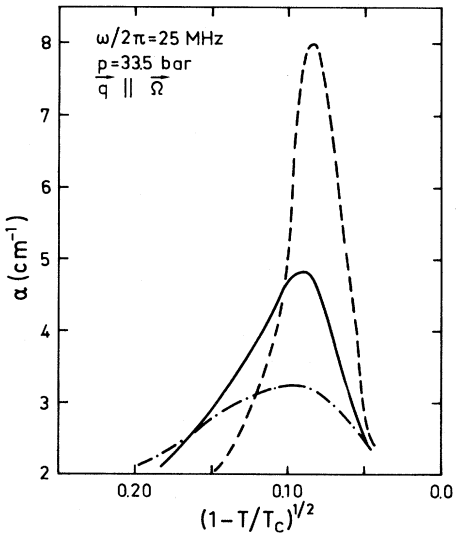

FIG. 7. Effective sound attenuation for the type-I (solid curve), $\hat{z}$ (dashed-dotted curve), and $\hat{x}$ (dashed curve) vortex lattices at $p=33.5$ bar and sound frequency of 25 Mhz with $\hat{q}\,||\,\vec{\Omega}$.

TABLE I. Elastic hydrodynamic parameters normalized to $\rho_{||}$ for ^{3}He-A at melting pressure (from Ref. 22).

T/T_c	$\bar{\rho}_s$	$\bar{\rho}_0$	$\bar{C}$	$\bar{C}_0$	$\bar{K}_s$	$\bar{K}_t$	$\bar{K}_b$	$\bar{K}_5$	$\bar{K}_6$	$\bar{K}'_s$	$\bar{K}'_t$	$\bar{K}'_b$	L_D (μm)
1.0	2.00	1.00	0.50	1.00	0.50	0.50	1.50	1.00	2.00	2.50	2.50	2.50	5.96
0.9	2.08	1.08	0.55	1.05	0.43	0.47	1.44	0.89	1.67	2.10	2.14	2.33	6.95
0.8	2.17	1.17	0.60	1.10	0.37	0.44	1.39	0.79	1.36	1.73	1.80	2.18	8.10
0.7	2.27	1.27	0.67	1.17	0.31	0.41	1.33	0.68	1.10	1.41	1.51	2.01	9.21

and $\hat{x}$-vortex lattices obtained using Wölfle and Koch's values of $\alpha_{||}$, α_c, and $\alpha_\perp$ at $\omega/2\pi=25$ Mhz and $p=33.5$ bar. The peak in the sound attenuation at $t^{1/2}\cong 0.10$ is due to the clapping mode of the order parameter, and the different strengths shown in Fig. 7 reflect the different weights multiplying $\alpha_\perp$ [Eqs. (61)] in which this mode appears. Thus, by calibrating $\alpha_\perp$ for $\Omega=0$ these changes in attenuation may be useful in identifying textures in rotating ^{3}He-A; experimental confirmation of the nonsingular vortex lattice would be most valuable.

Experimental studies of rotating ^{3}He-A (Ref. 29) have relied on NMR, necessitating a large magnetic field ($H\sim 300$ Oe), that qualitatively alters the vortex texture from that considered here. Although theoretical estimates indicate that singular vortices have lower energy in such fields,[30–32] the observed[33] transverse NMR satellite (frequency shift and intensity) suggests that nonsingular $p=2$ vortices are actually created. More research will be needed to resolve this discrepancy.

ACKNOWLEDGMENTS

This research was supported in part by the National Science Foundation, under Grants Nos. DMR-81-18386 (A.L.F.) and DMR-80-2063 (J.A.S. and D.L.S.). J.A.S and D.L.S. thank the Aspen Center for Physics, where part of this work was performed.

APPENDIX

The dipole-locked bending coefficients in Eq. (30b) are related to the dipole-unlocked bending coefficients in Eq. (30a).

$$K'_s=K_s+K_6\ ,\quad K'_t=K_t+K_6,$$
$$K'_b=K_b+K_5,\quad K'_4=K_4-K_6\ . \tag{A1}$$

For $T\simeq T_c$ all of the hydrodynamic parameters can be related to the A-phase gap $\Delta(T)$ and the GL coefficients in Eq. (29d),

$$\rho_s=K_6=4\Delta^2(K_2+\tfrac{1}{2}K_1+\tfrac{1}{2}K_3)\ ,\quad C=2\Delta^2K_1\ ,$$
$$\rho_0=C_0=2\Delta^2(K_1+K_3)\ ,\quad K_s=K_t=-K_4=\tfrac{1}{2}K_5=2\Delta^2K_2\ , \tag{A2}$$
$$K_b=2\Delta^2(K_1+K_2+K_3),$$
$$K'_s=K'_t=K'_b=-K'_4=2\Delta^2(3K_2+K_1+K_3)\ .$$

In the weak-coupling BCS theory the GL parameters satisfy $K_1=K_2=K_3$. Thus for $T\simeq T_c$ the BCS values for the hydrodynamic parameters become

$$\bar{\rho}_s=\bar{K}_6=2,\quad \bar{K}_s=\bar{K}_t=-\bar{K}_4=\tfrac{1}{2}\bar{K}_5=\tfrac{1}{2}\ ,$$
$$\bar{C}=\tfrac{1}{2},\quad \bar{K}_b=\tfrac{3}{2}\ , \tag{A3}$$
$$\bar{\rho}_0=\bar{C}_0=1,\quad \bar{K}'_s=\bar{K}'_t=\bar{K}'_b=-\bar{K}'_4=\tfrac{5}{2}\ ,$$

where $\bar{x}\equiv x/\rho_{||}$ and $\rho_{||}\equiv\rho_s-\rho_0$.

For lower temperatures, Williams[22] has tabulated the weak-coupling hydrodynamic parameters including Fermi-liquid effects. The temperature-dependent hydrodynamic parameters used in this paper are given in Table I.

[1]G. E. Volovik and V. P. Mineyev, Zh. Eksp. Teor. Fiz. 72, 2256 (1977) [Sov. Phys.—JETP 45, 1186 (1977)].
[2]N. D. Mermin, Rev. Mod. Phys. 51, 591 (1979).
[3]P. W. Anderson and G. Toulouse, Phys. Rev. Lett. 38, 508 (1977).
[4]T. Fujita, M. Nakahara, T. Ohmi, and T. Tsuneto, Prog. Theor. Phys. 60, 671 (1978).
[5]N. D. Mermin and T.-L. Ho, Phys. Rev. Lett. 36, 594 (1976).
[6]L. J. Buchholtz and A. L. Fetter, Phys. Rev. B 15, 5225 (1977).
[7]M. R. Williams and A. L. Fetter, Phys. Rev. B 20, 169 (1979).
[8]N. Schopohl, J. Low Temp. Phys. 41, 409 (1980).
[9]We measure velocities in units of inverse length. The factor $\hbar/m_4$ ($\hbar/2m_3$ for ^{3}He) in the usual definition of $\vec{v}_s$ is included implicitly in the free energy.
[10]R. P. Feynman, Prog. Low Temp. Phys. I, 17 (1955).
[11]V. K. Tkachenko, Zh. Eksp. Teor. Fiz. 49, 1875 (1965) [Sov. Phys.—JETP 22, 1282 (1966)].
[12]See, for example, N. D. Mermin, in *Quantum Liquids*, edited by J. Ruvalds and T. Regge (North-Holland, Amsterdam, 1978), p. 195.
[13]We use the conventions of A. R. Edmonds, *Angular Momentum in Quantum Mechanics* (Princeton University Press, Princeton, N. J., 1957), p. 6.
[14]See, for example, T.-L. Ho, Ph.D. thesis, Cornell University, 1978 (unpublished).
[15]W. F. Brinkman and M. C. Cross, Prog. Low Temp. Phys. VIIA, 105 (1978).
[16]A. L. Fetter, Phys. Rev. B 20, 303 (1979).
[17]T. Passvogel, N. Schopohl, M. Warnke, and L. Tewordt, J. Low Temp. Phys. 46, 161 (1982), have evaluated the next corrections in powers of $1-T/T_c$.
[18]G. E. Volovik and N. B. Kopnin, Zh. Eksp. Teor. Fiz. Pis'ma

Red. 25, 26 (1977) [Sov. Phys.—JETP Lett. 25, 22 (1977)].
[19]See, for example, N. W. Ashcroft and N. D. Mermin, *Solid State Physics* (Holt, Rinehart and Winston, New York, 1976), Chap. 4.
[20]M. Abramowitz and I. A. Stegun, *Handbook of Mathematical Functions* (U.S. Dept. of Commerce, Washington, D.C., 1964), Chap. 18.
[21]P. Muzikar, J. Phys. (Paris) Colloq. 39, C6-53 (1978). See also F. Fishman and I. A. Privorotskii, J. Low Temp. Phys. 25, 225 (1976).
[22]Mark Williams, Ph.D. thesis, Stanford University, 1979 (unpublished); see also Ref. 16.
[23]G. E. Volovik and P. J. Hakonen, J. Low Temp. Phys. 42, 503 (1981).
[24]M. Nakahara, T. Ohmi, T. Tsuneto, and T. Fujita, Prog. Theor. Phys. 62, 874 (1979).
[25]J. W. Serene, Ph.D. thesis, Cornell University, 1974 (unpublished).
[26]P. Wölfle and V. E. Koch, J. Low Temp. Phys. 30, 61 (1978).
[27]D. N. Paulson, R. T. Johnson, and J. C. Wheatley, Phys. Rev. Lett. 31, 746 (1973).
[28]The effective attenuation defined by $\exp(-\bar{\alpha}L) = A_{\text{cell}}^{-1} \int d\vec{r} \exp[-\alpha(\vec{r})L]$ is valid in the limit $2\pi/q \ll a$. This condition is satisfied up to distances of order $a \sim 3L_D$ for $\omega/2\pi \gtrsim 25$ Mhz at melting pressure. In addition, Eqs. (61) are valid for $\alpha_{\max}L \ll 1$; however, numerical calculations show that Eqs. (61) are reasonably good for $\alpha_{\max}L \lesssim 5$, where L is the path length between the sound transmitter and receiver.
[29]P. J. Hakonen, O. T. Ikkala, and S. T. Islander, Phys. Rev. Lett. 49, 1258 (1982).
[30]H. K. Seppälä and G. E. Volovik, J. Low Temp. Phys. 51, 279 1983).
[31]K. Maki, Phys. Rev. B 27, 4173 (1983).
[32]V. Vulovic (private communication).
[33]P. J. Hakonen, O. T. Ikkala, S. T. Islander, O. V. Lounasmaa, and G. E. Volovik, J. Low Temp. Phys. (in press).